

Simulating the Galactic Centre: A Comparison of Medium-Sized Telescopes and Schwarzschild-Couder Telescopes

Anna Wong

Saturday 5th August, 2023

Abstract

The Galactic Centre has a high density of interesting gamma-ray sources, including several supernova remnants, dense star-forming regions, and the nearest black hole. In order to improve the resolution of its images of this region, it has been proposed that CTAO add 11 Schwarzschild-Couder telescopes to their southern array. The dual-mirrored design of these telescopes corrects for aberrations and results in clearer images, making it easier to both distinguish between sources and study individual source morphology. This investigation simulates gamma ray event data from the Galactic Centre with and without SCTs, demonstrating their importance to CTAO's southern array.

Contents

1	Introduction1.1 Imaging Atmospheric Cherenkov Technique1.2 Cherenkov Telescope Array Observatory1.3 Schwarzschild-Couder Telescopes	3
2	Method	7
3	Results 3.1 Sagittarius A* image of hadronic gamma ray emission	
4	Further investigation	14
5	Conclusion	15
6	Acknowledgements	16

1 Introduction

The means by which cosmic rays are accelerated is a major question in high-energy astrophysics. Supernova remnants, which are considered to be one of the primary Galactic cosmic ray sources, are proposed to accelerate particles via a process called diffusive shock acceleration (1). Because the shock waves that spread from a supernova are not completely uniform, particles caught between moving electromagnetic inconsistencies can 'ping-pong' between them as seen in Figure 1, gaining kinetic energy until they have enough to overcome the shock front.

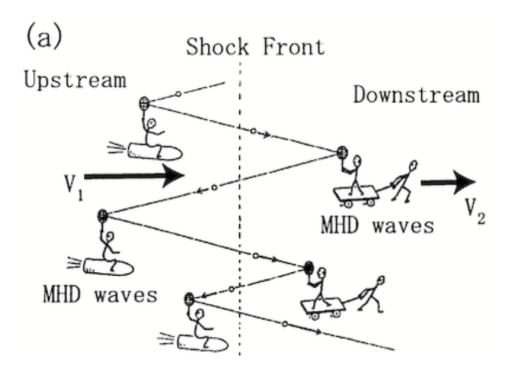


Figure 1: Cartoon of a particle gaining energy from the magneto-hydrodynamic waves generated by a supernova (2)

The means by which cosmic rays emit gamma rays depends on the type of particle it is. If the particle is a proton, it may interact with other protons in the environment and produce neutral pions which will decay into photons (1). Cosmic ray sources that are near molecular clouds are consequently more likely to indirectly emit these photons. If the particle is an electron, then it may undergo inverse Compton scattering, transferring its energy to low-energy photons in the cosmic microwave background and scattering them. Both interactions produce high-energy gamma rays, which can then travel unimpeded to Earth's atmosphere. Protons and electrons themselves can also reach Earth's atmosphere, but since they may have been deflected by Galactic magnetic fields, their origin cannot be reconstructed as accurately.

Upon entering Earth's atmosphere, both gamma rays and cosmic rays undergo a series of particle interactions with atmospheric nuclei, creating gamma-ray air showers. The two different processes that can occur are pictured in Figure 2.

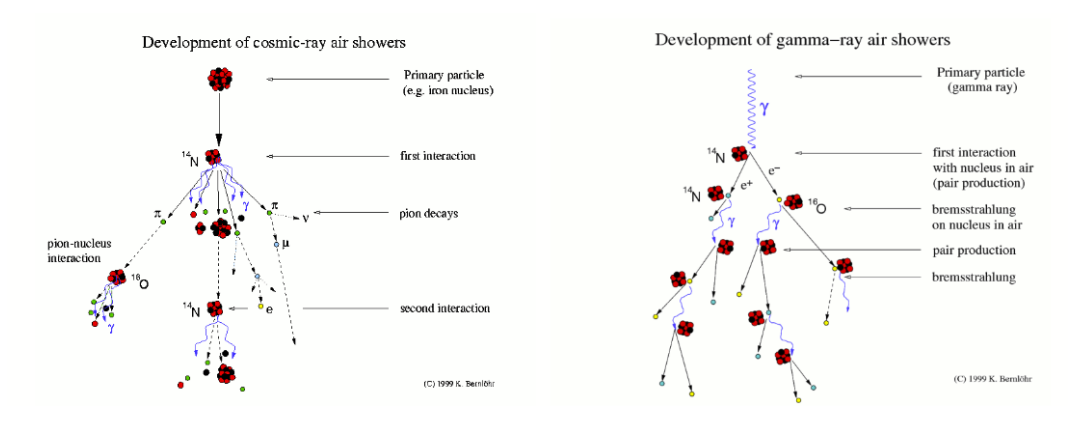


Figure 2: How relativistic cosmic and gamma rays produce gamma ray airshowers in the atmosphere (3)

These gamma rays are superluminal in the medium, creating bursts of light analogous to that of a supersonic jet's 'sonic boom'. Known as Cherenkov radiation, they only last a few nanoseconds and cannot be seen by the human eye. However, as the photons reach the ground, they can be imaged by ground telescopes using the Imaging Atmospheric Cherenkov Technique (IACT), as shown in Figure

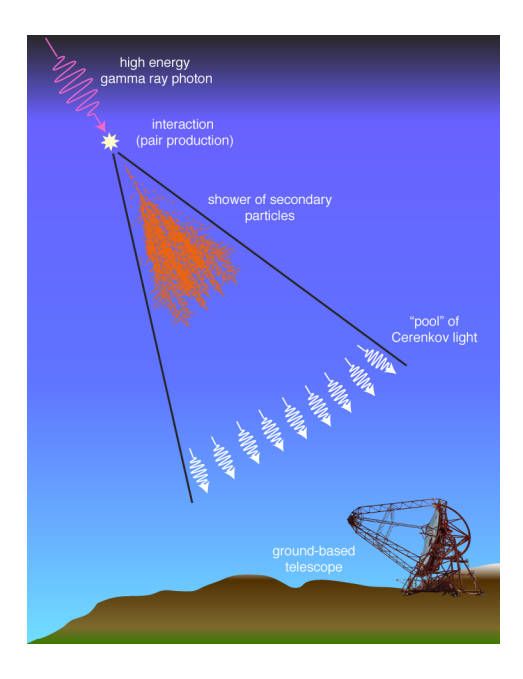


Figure 3: An illustration of the 'light pool' created by an air shower.(4)

1.1 Imaging Atmospheric Cherenkov Technique

The Imaging Atmospheric Cherenkov Technique (IACT) uses the Cherenkov light from gamma-ray showers to triangulate sources of high-energy gamma rays. Large, mirrored dishes are used to reflect light from air showers at cameras as seen in Figure 4. Examples of an individual telescope's airshower image are shown in Figure 9. The shower images are parameterized using Hillas parameters (5), and these parameters are used to reconstruct the energies and the directions of the air showers.

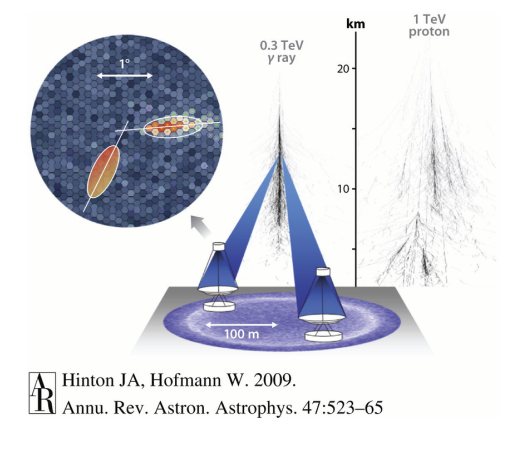


Figure 4: An illustration of the images from two telescopes in an IACT array being combined to triangulate an airshower's origin (6)

1.2 Cherenkov Telescope Array Observatory

The Cherenkov Telescope Array Observatory (CTAO) is the next-generation observatory for high-energy astronomy utilizing the IACT technology. It will cover large swathes of land to maximize the potential for imaging rare high-energy gamma rays. There will be a large, medium, and small size for the telescopes, pictured in Figure 5. These different sizes are designed to detect different energy ranges

(20 to 150 GeV, 150 GeV to 5 TeV, and 5 to 300 TeV respectively) (7). Consequently, the CTAO will be able to cover a very wide range of gamma-ray energies.

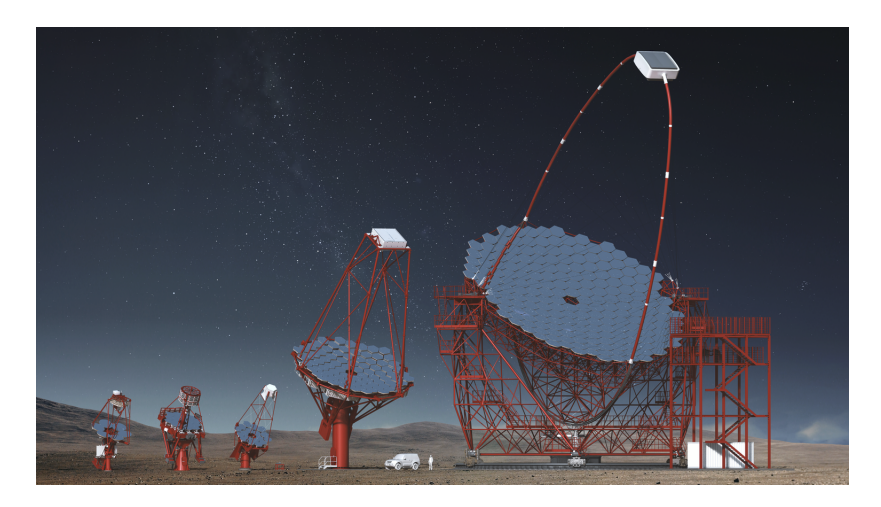


Figure 5: From left to right: CTAO's small-sized, medium-sized, and large-sized telescopes (7)

The observatory will consist of two telescope arrays. The northern hemisphere array in La Palma, Spain will cover low- to mid-energy events (20 GeV to 5 TeV) while the southern hemisphere array in the Atacama Desert near Paranal, Chile will cover mid- to high-energy events (150 GeV to 300 TeV) (8). The southern array will cover the center of our galaxy, an area dense with cosmic ray sources. Since the imaging of this region has great potential to advance high-energy astrophysics, the augmentation of the southern array with higher-resolution telescopes has been proposed.

1.3 Schwarzschild-Couder Telescopes

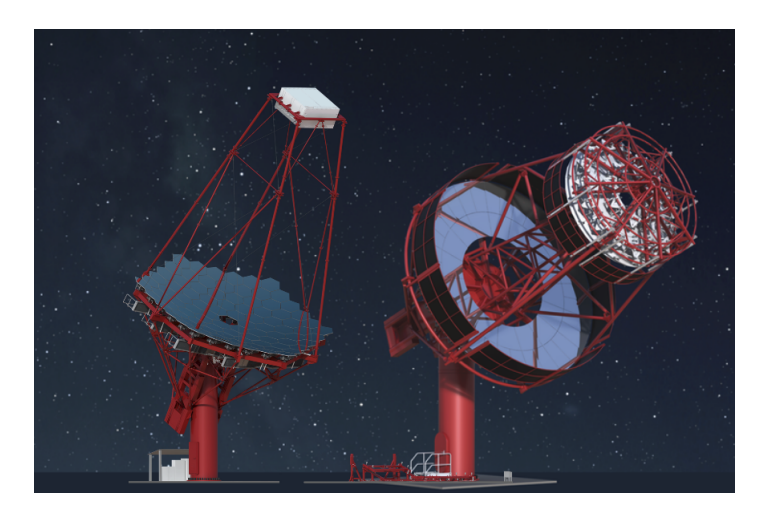


Figure 6: CTAO's medium-sized telescope (left) and a Schwarzschild-Couder telescope (right) (7)

The CTAO's design for their medium-sized telescopes (MSTs) uses a Davies-Cotton system, which are reliable for smaller sources but which suffer from comatic aberrations for larger fields of view (9). The mirror fails to properly reflect airshowers that are offset from the optical axis, causing spherical aberrations. This is evident in Figure 7. In contrast, Schwarzschild-Couder Telescopes (SCTs) pictured in Figure ?? feature a dual-mirrored design that corrects for aberrations as demonstrated in Figure 8.

This design maintains a point spread function of 3.2 arc-minutes across the SCT's entire field of view, meaning that the clarity of the SCT's images do not degrade towards their edges as much as the MST's do. It also de-magnifies the image, allowing compact silicon photomultipliers instead of

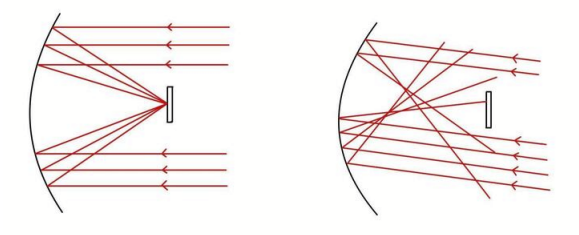


Figure 7: When airshowers aren't perpendicular to the MST's mirror, only a small part of the image is usable.

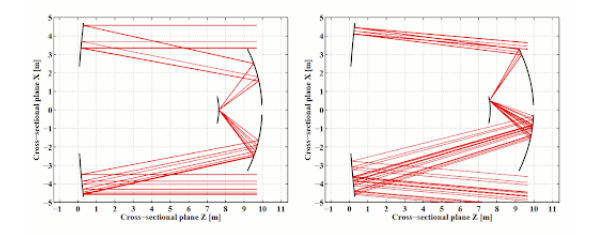


Figure 8: Regardless of where or at what angle light hits the primary mirror, the secondary mirror of a SCT can re-reflect it to a single focal point.

photomultiplier tubes (10). The resulting images thus have a much higher pixel density than the MST. This wider effective field of view and higher resolution can be see in Figure 9.

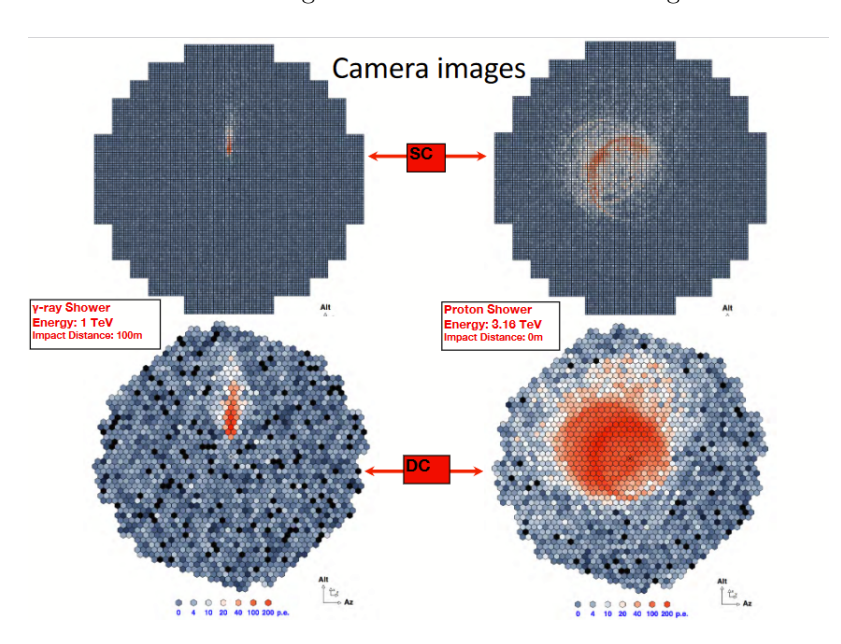


Figure 9: Camera images from a MST and SCT of both a gamma ray and cosmic ray airshower. The SCT provides a much clearer image of both.

The current configuration that CTAO has planned for their southern hemisphere array (their Alpha configuration) currently includes 14 MSTs. However, the Alpha-V2 configuration pictured in Figure 10 would include 11 SCTs, greatly improving the array's imaging capabilities.

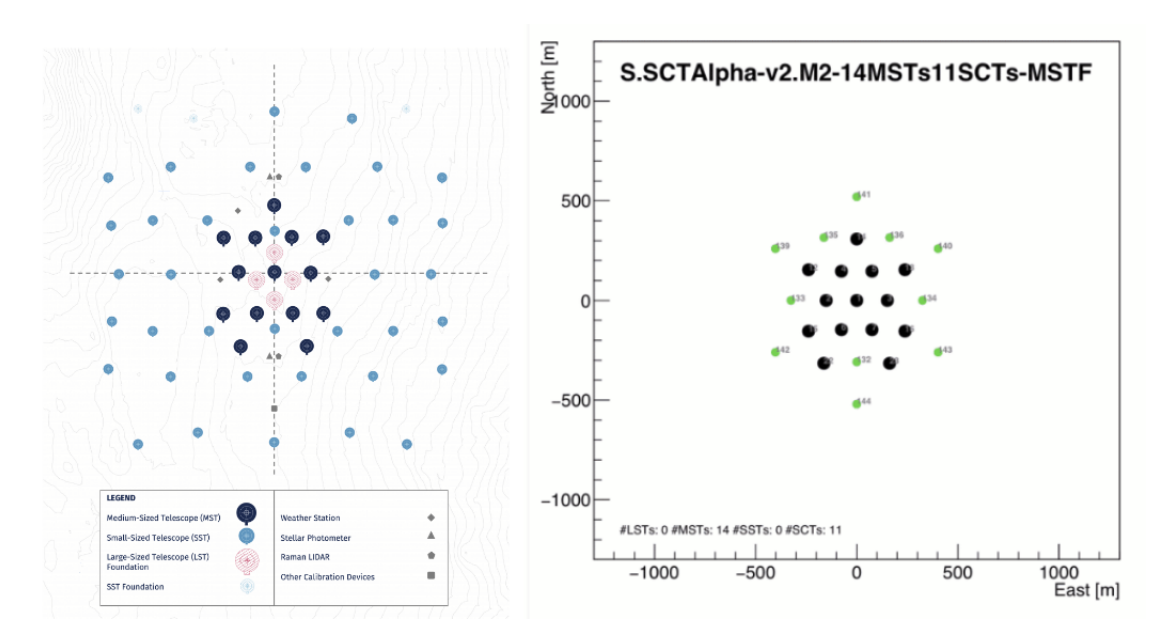


Figure 10: Left: The current Alpha configuration of the southern array. Right: The Alpha-V2 configuration, which includes 11 SCTs (green) in addition to the 14 MSTs. The small-sized telescopes are not pictured. (8)

This improvement would be especially relevant to the CTAO's imaging of the Galactic Centre, which has a high density of cosmic ray sources. Of particular interest is a single very-high energy source which may be connected to Sagittarius A*, the nearest black hole; however, there are also several SNRs, pulsar wind nebulae, and molecular clouds that are worth investigating. Because these sources are clustered together (and because several of them are quite small and will be hard to resolve), a high angular resolution would greatly benefit CTAO's imaging of the area. My project aims to demonstrate the importance of adding SCTs to CTAO's southern array to better resolve sources of high-energy cosmic rays in the Galactic Centre.

2 Method

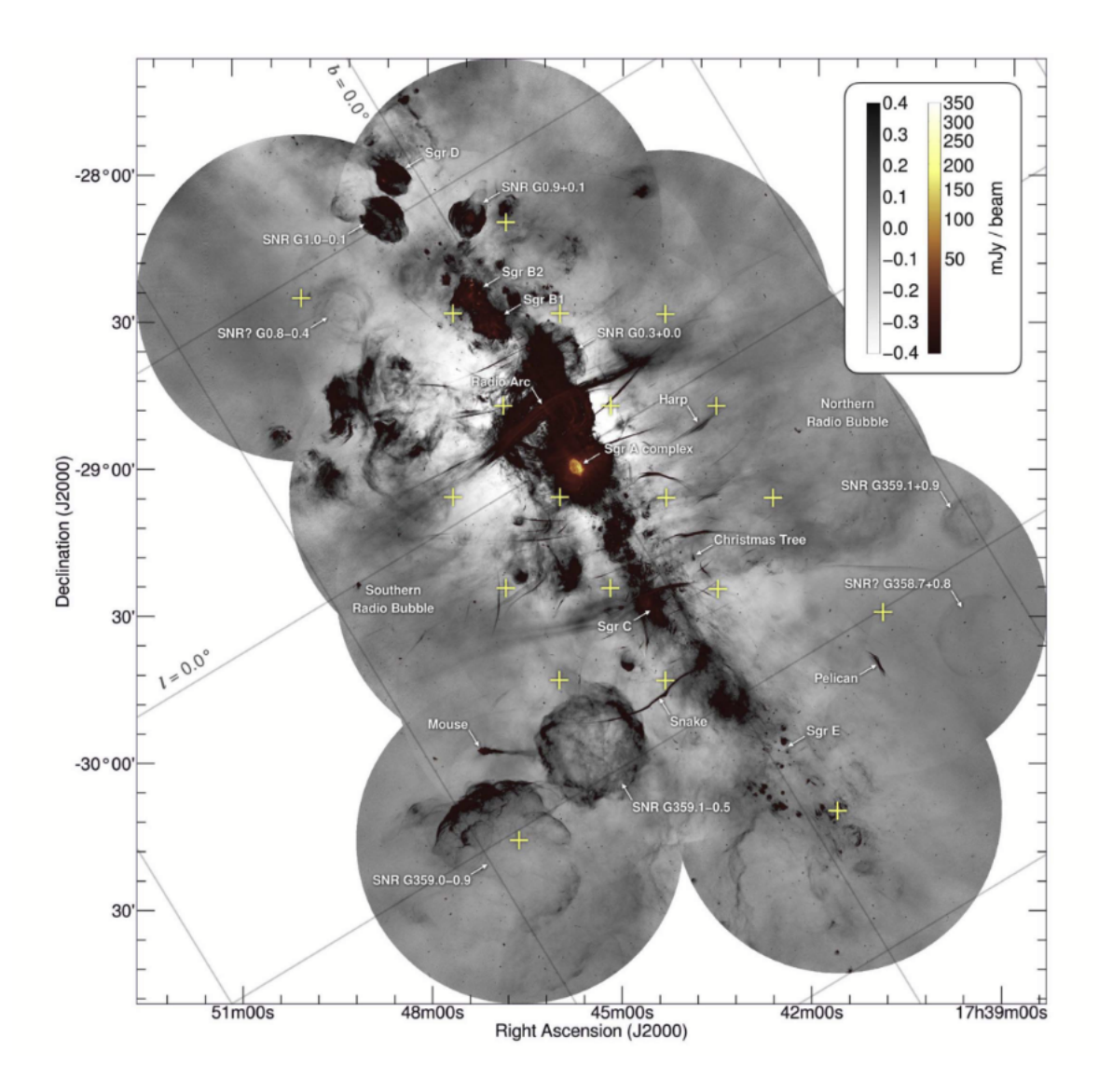


Figure 11: A mosaic of Galactic Centre, consisting of twenty pointings from the South African MeerKAT radio telescope. This data is the foundation of my gamma ray event simulation (11)

As mentioned in Section One, the ability of gamma rays to travel through the interstellar medium without being deflected by magnetic fields makes them very useful in the investigation of SNRs as cosmic accelerators. Since matter is required for gamma ray production, SNRs near denser structures such as molecular clouds are expected to produce a higher flux of gamma rays (12). This has been seen in the Galactic Center, where "The diffuse [gamma-ray] emission spatially correlates with the inner dense clouds" of near Sagittarius A* (13).

The following two equations from Aharonian et al. (12) give the relationship between gamma ray flux and the density of a nearby cloud through the factor A:

$$F_{\gamma}(\geq E) = (f_{\alpha} \times 10^{-10}) \left(\frac{E^{-\alpha+1}}{1\text{TeV}}\right) (A) \tag{1}$$

in which E is the energy of the gamma rays, $f_{\alpha} \times 10^{-10}$ is a constant that approximates the proton-proton cross-section of a hadronic collision ($f_{\alpha} \sim 1$), α is the spectral index of protons, and A is

provided by the following equation:

$$A = \theta \left(\frac{E_{SN}}{10^{51} \text{erg}}\right) \left(\frac{1 \text{kpc}}{d}\right)^2 \left(\frac{n}{1 \text{cm}^3}\right),\tag{2}$$

in which θ is the fraction of total SNR energy converted to cosmic rays, E_{SN} is the total explosion energy of the supernova, d is the distance to the SNR, and n is the density of hydrogen atoms surrounding the SNR. The first two terms simplify to E_{CR} , the total cosmic ray energy from the SNR. Since this investigation assumes a constant diffuse cosmic ray flux, the volume V in the denominator of n can be moved to the denominator of E_{CR} . The equation is now:

$$A = \left(\frac{E_{CR}}{V}\right) \left(\frac{1\text{kpc}}{d}\right)^2 (N_{total})$$

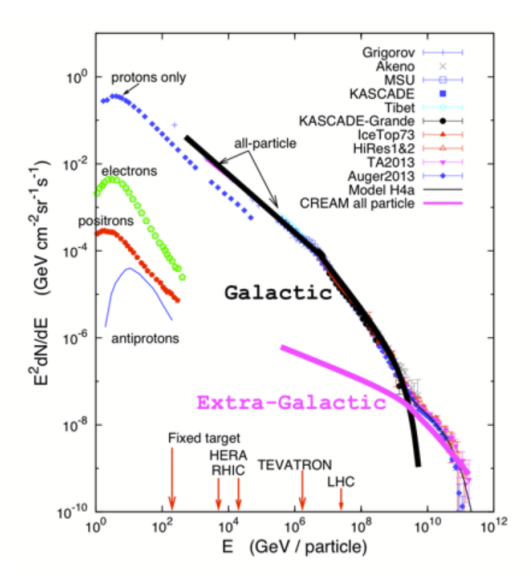


Figure 12: A graph of cosmic ray energies versus flux. The changes in slope at $E=10^{16}$ and 10^{19} are referred to as the 'knee' and 'ankle' respectively, and the causes for these changes is unknown

The energy range of interest for gamma rays is around 1 TeV, the range that MSTs and SCTs detect energy at. Since hadronic cosmic rays only transfer about 1/10 of their energy to gamma rays when they interact with other hadrons (14), a cosmic ray energy of 1 TeV × 10, i.e. 10^4 GeV, can be assumed. The cosmic ray flux at this energy is of the order of 10^{-2} GeV/cm²/s (see Figure 12). $\frac{E_{CR}}{V}$ can be found using the definition of flux, $F = \frac{E}{a\Delta t}$:

$$\frac{E_{CR}}{V} = \frac{E_{CR}}{a \times L} = \frac{E_{CR}}{a \times (c\Delta t)} = \frac{E_{CR}}{c(a \times \Delta t)} = \frac{F_{CR}}{c}$$
(3)

where a and L are the area and depth of the volume V and c is the speed of light. The only variable left is the hydrogen column density in the medium surrounding the SNR, n. This can be found using the Galactic Centre mosaic from the South African MeerKAT radio telescope 11, which is an image of the Galactic Centre's spectral flux density (11). Assuming that the radiation has a wavelength of 21 cm (i.e. the hydrogen line, a spectral line commonly used in radio astronomy for the detection of hydrogen), then the following equation (15) can be used to convert spectral flux density to column density for sources with no redshift:

$$N_{H1} \approx (2.33 \times 10^{20})(\theta^{-2}) \int Sdf$$
 (4)

in which N_{HI} is the hydrogen column density, z is the redshift, θ is the telescope's beam width in arcseconds, and $\int Sdf$ is the spectral flux density integrated over the telescope's detected frequencies.

The spectral flux density is provided by the mosaic itself, and the MeerKAT data band width is $\Delta f = 800$ MHz. Using this equation, the area surveyed by the MeerKAT mosaic has approximately 8×10^{66} hydrogen atoms.

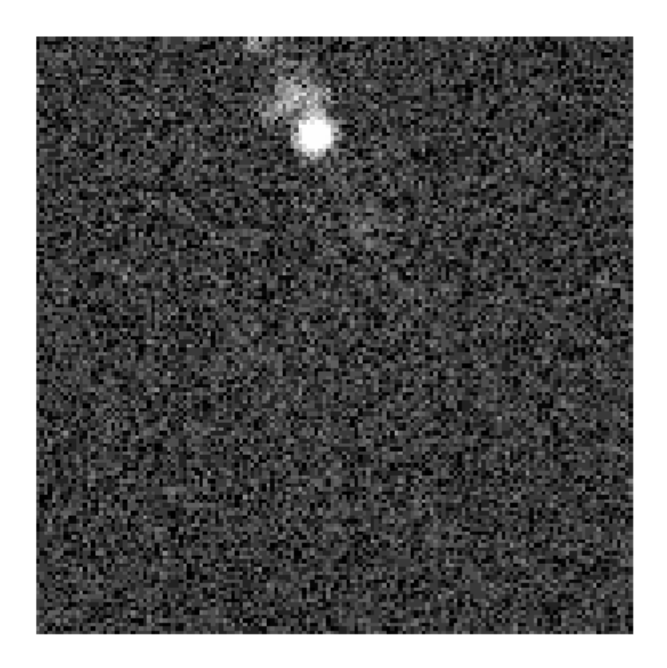
Combining Equation3 and Equation4, A is thus 1.54×10^{-17} .

I used ctools, a software package designed for gamma ray image analysis, to simulate the gamma ray flux from the Galactic Centre using A to normalize the power law spectrum. The simulations were of three different configurations: one using 14 MSTs, the second using 14 MSTs and 11 SCTs, and the third using a configuration with 25 MSTs as a control. Any increase in the number of telescopes will create a higher resolution image; the 25 MST configuration demonstrates the effect that the SCTs will have specifically.

3 Results

3.1 Sagittarius A* image of hadronic gamma ray emission

The following images are the result of a ten-hour pointing at the Galactic Centre. Each image covers approximately 3×3 degrees of sky. The only visible cosmic ray source is Sagittarius A* and the Radio Arc above it.



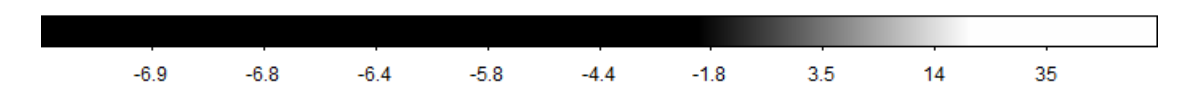


Figure 13: Simulated gamma-ray event data from 14 MSTs with simulated background subtracted. Sagittarius A* overwhelms@articlearticle, author = Nieto, D.Y. and Griffiths, S. and Humensky, Brian and Kaaret, Philip and Limon, M. and Mognet, I. and Peck, A. and Petrashyk, A. and Ribeiro, Dora and Roussselle, Julien and Stevenson, B. and Vassiliev, V. and Yu, Peijiong and Consortium, for, year = 2015, month = 09, pages = , title = Construction of a medium-sized Schwarzschild-Couder telescope as a candidate for the Cherenkov Telescope Array: development of the optical alignment system the image

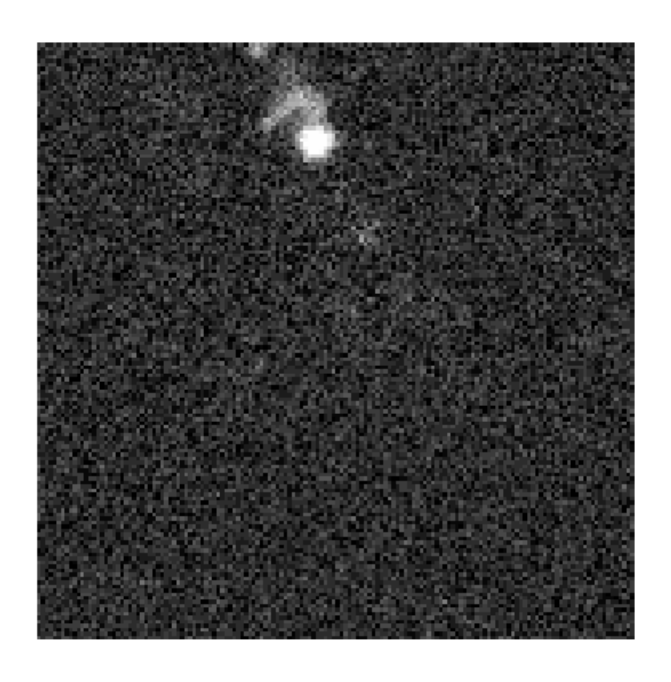




Figure 14: Simulated gamma-ray event data from 14 MSTs and 11 SCTs with simulated background subtracted

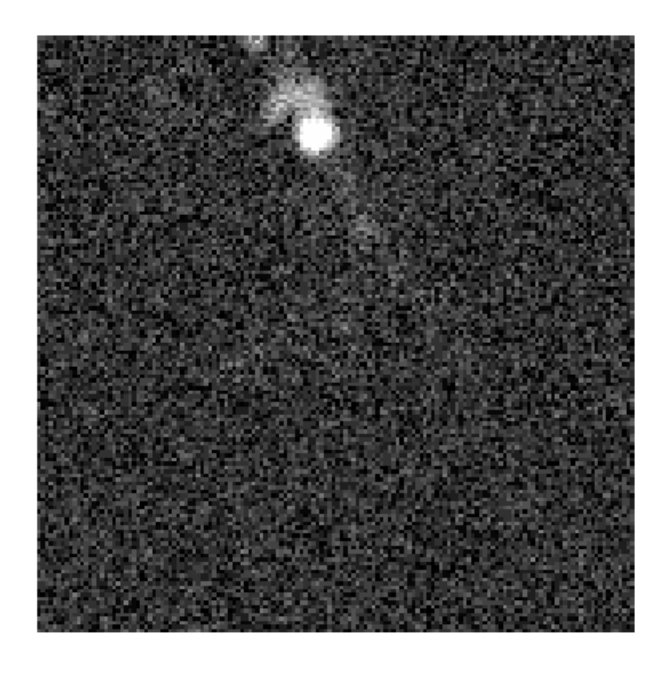




Figure 15: Simulated gamma-ray event data from 25 MSTs with simulated background subtracted

Even though other sources were washed out by Sagittarius A*, slight improvements from the inclusion of the SCTs are still visible. The Radio Arc is more clearly defined and the edges of Sagittarius A* are better delineated from the background in Figure 14. While 25 MSTs seems to be an improvement from 14 MSTs, it still does not create as dramatic of a change in clarity as the 11 SCTs. As seen in the colorbars of each image, the array with 11 SCTs included was also able to image more events than both the 14 MST array and the 25 MST array.

3.2 Hadronic gamma ray emission from molecular cloud structures near Sagittarius A^*

There are several features of interest in the Galactic Centre other than Sagittarius A*. In addition to several supernova remnants, Sagittarius B1 is a region dense with over a hundred thousand solar masses of young stars and Sagittarius C is an extremely dense molecular cloud. All three are potential sources of hadronic gamma rays. In order to see these other sources in the Galactic Centre, it was necessary to mask Sagittarius A* in the MeerKAT data ((seen in Figure 16). Using the masked version, I ran a twenty-hour pointing at the Galactic Centre with the same three configurations of telescopes.

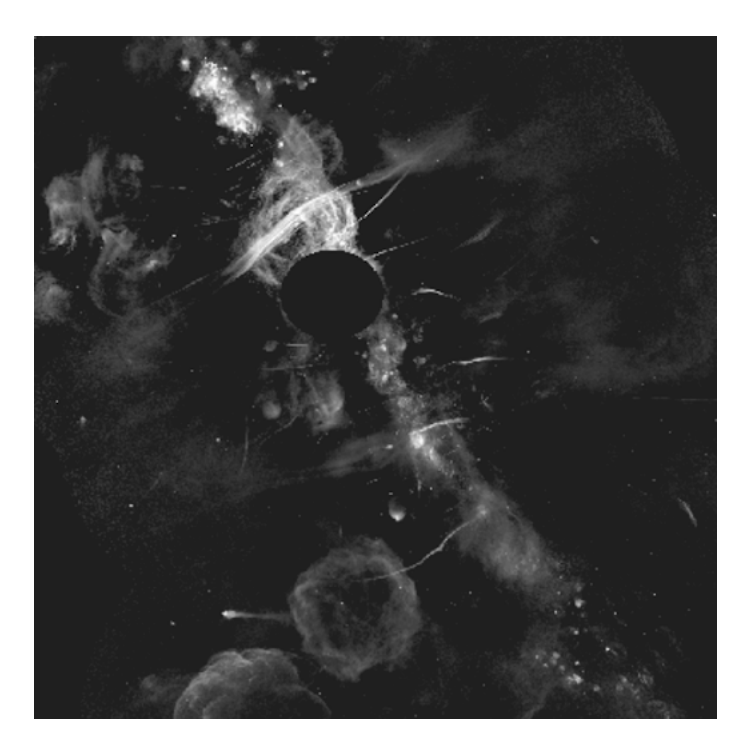


Figure 16: The masked version of the MeerKAT data

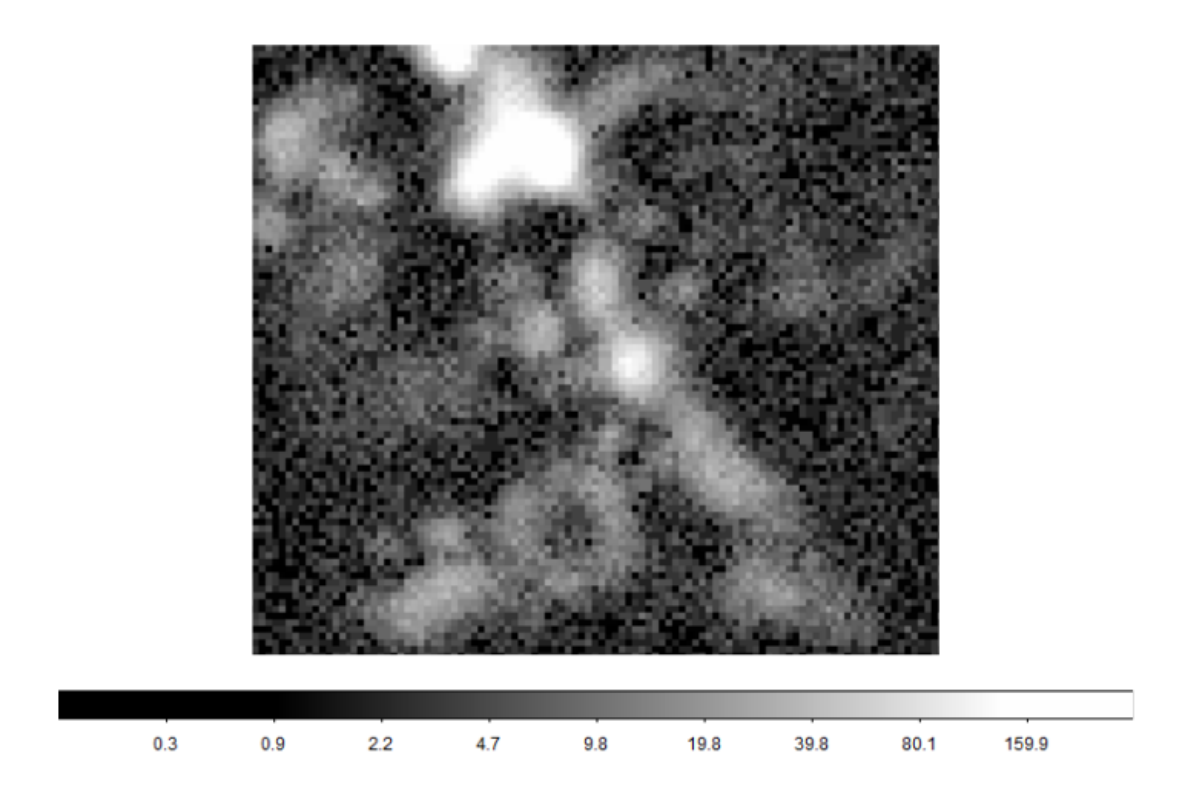


Figure 17: An image of simulated gamma ray events using an array of 14 MSTs. The event counts are indicated by the color bar at the bottom

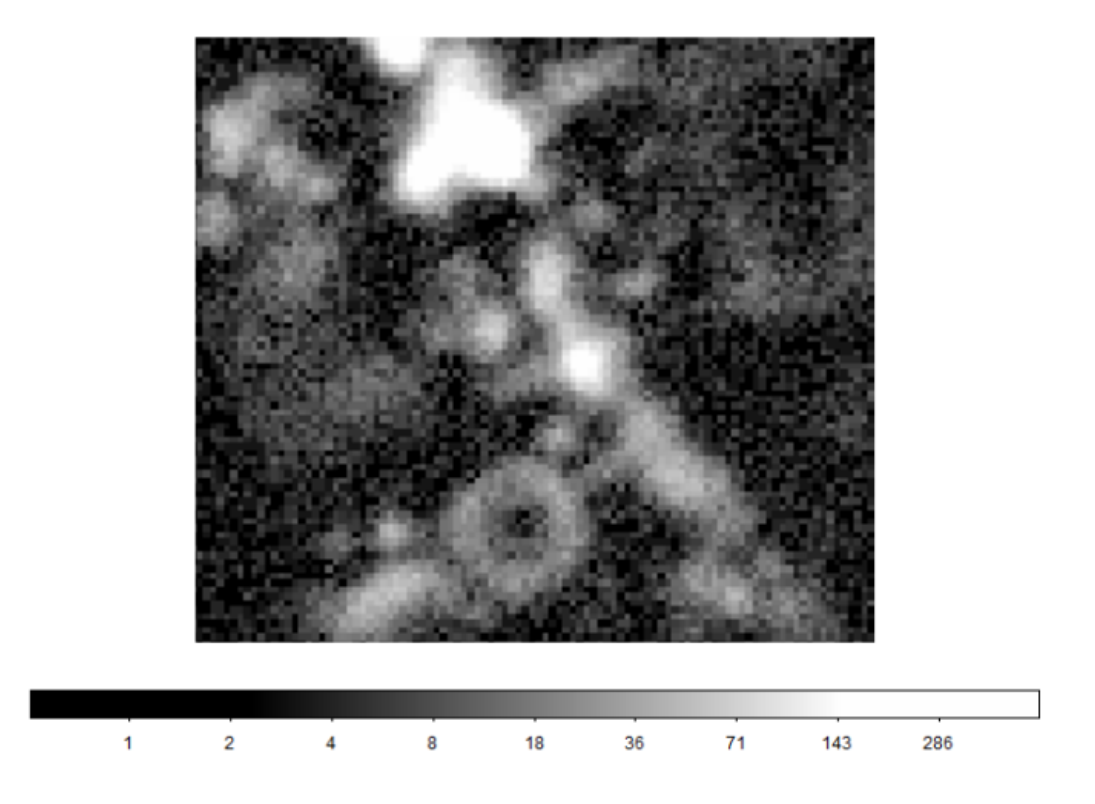


Figure 18: An image of simulated gamma ray events using an array of 25 MSTs. This is meant to act as a 'control'; any increase in the number of telescopes will yield a higher-resolution image, but there is still a noticeable difference between this image and Figure 19

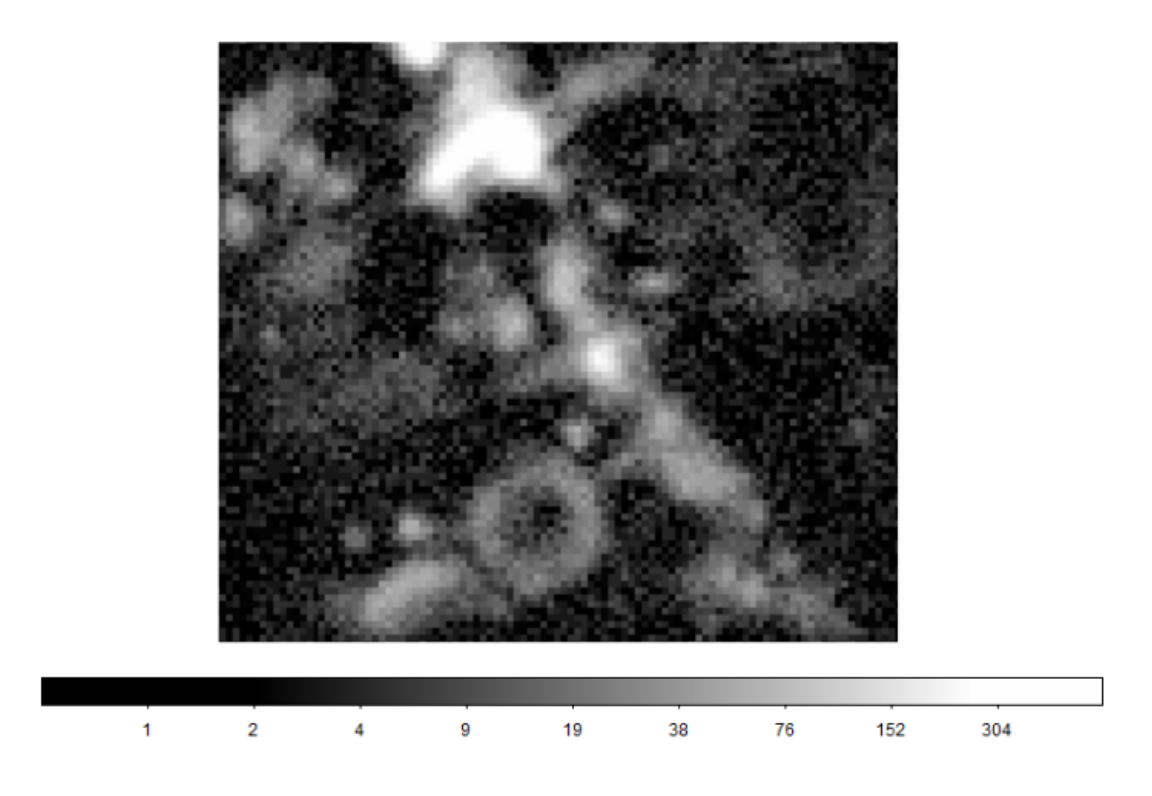


Figure 19: An image of simulated gamma ray events using an array of $14~\mathrm{MSTs}$ and $11~\mathrm{SCTs}$

The round black shape between Sgr B1 and Sgr C is the result of the mask, but other features of the Galactic Centre such as Sgr B1, Sgr C, SNR 359.1-0.5, a part of SNR 359.0-0.9, and the Christmas Tree are still clear.

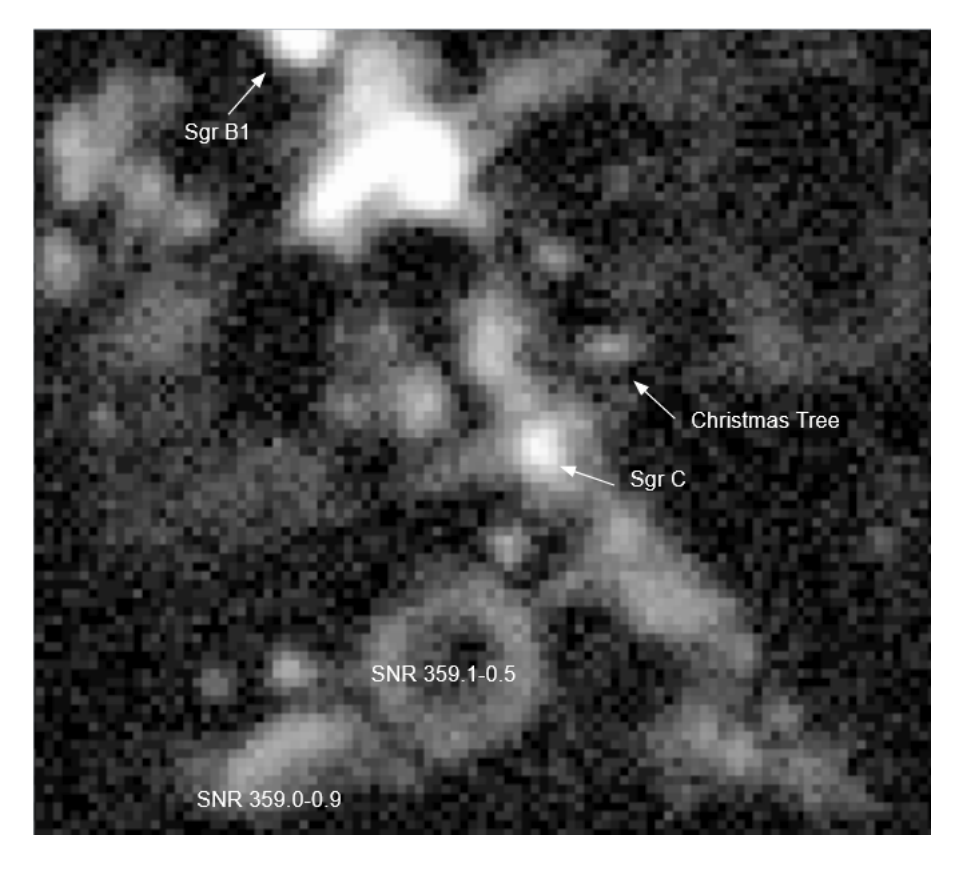


Figure 20: The image from 14 MSTs and 11 SCTs with features from the MeerKAT mosaic labelled

From Figures 18 and 19 it is immediately apparent that the configuration with the SCTs created an image with clearer differentiation between sources. The shell surrounding SNR 359.1-0.5 is more distinct with 11 SCTs than it is with 25 MSTs; with only 14 MSTs, not only is the shell much 'fuzzier', but the structures surrounding the SNR almost blend into it. Additionally, the morphology around Sagittarius C is more clearly defined with the 11 SCTs. The Christmas Tree, for example, is seen as more elliptical with the SCTs, while it is only vaguely round with the MSTs. It's also worth noting that the SCT array was able to detect nearly twice as many events as the 14 MSTs, providing much more data with the same duration of pointing.

4 Further investigation

This report assumes that there is a uniform flux of cosmic rays interacting with the molecular clouds observed in the MeerKAT data, creating a gamma-ray image that mirrors the distribution of molecules. However, there is also the "local" cosmic ray flux produced by individual SNRs that can only illuminate nearby clouds. The next step of this research would be to consider the local flux by assuming a particle diffusion model in the presence of the interstellar magnetic field. For example, Figure 22 has a Gaussian scale applied to it such that flux is inversely correlated with distance.

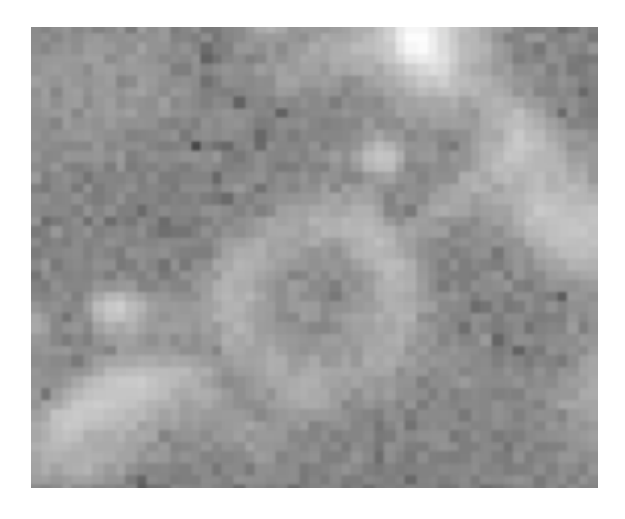


Figure 21: Simulated gamma ray events from SNR359.1-0.5

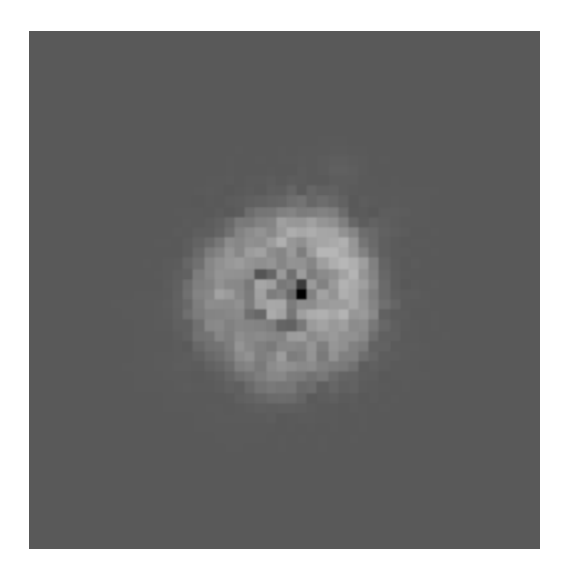


Figure 22: SNR359.1-0.5 with a Gaussian function applied such that the cosmic ray flux is higher at the center of the shell

5 Conclusion

The IACT allows the investigation of ultra-high energy cosmic ray sources by detecting the gamma ray emission from the interactions between cosmic rays and molecular clouds near the source. With 11 SCTs added to their southern array, the CTAO's findings would be at the very forefront of astroparticle physics. Better images of these particle accelerators and their morphologies will translate into a better understanding of both the astronomy and the physics behind these sources. The SCT's higher resolution could lead to the discovery of new cosmic ray sources and distinguish between known ones (10). Furthermore, by resolving the details of accelerators' morphologies, astronomers will be able to learn more about these sources' acceleration mechanisms. These mechanisms are relevant to particle physicists, as the extraordinary environments of the Galactic Centre provide an opportunity to study high-energy physics well beyond any environment that could be created on Earth. High-energy physics stands to gain much from the addition of 11 SCTs to the CTAO's southern array.

6 Acknowledgements

I would like to thank Professor Reshmi Mukherjee, Dr. Ruo Shang, and the rest of the VERITAS group at Columbia and Barnard for their guidance and support of my research this summer. I'd also like to thank Amy Garwood, Professor Georgia Karagiorgi, and Professor John Parsons for the opportunity to do research at Nevis Labs, and for their support of Columbia's REU program. This material is based upon work supported by the National Science Foundation under Grant No. PHY/950431.

References

- [1] D. Caproili R. Giuffrida, M. Miceli et al. The supernova remnant sn 1006 as a galactic particle accelerator. *Nature Communications*, 13, 2022.
- [2] Masahiro Hoshino. Nonthermal particle acceleration in shock front region: Shock surfing accelerations. Progress of Theoretical Physics Supplement PROG THEOR PHYS SUPPL, 143:149–181, 05 2001. doi: 10.1143/PTPS.143.149.
- [3] Konrad Bernlöhr. Cosmic-ray air showers. URL https://www.mpi-hd.mpg.de/hfm/CosmicRay/Showers.html.
- [4] Gamma-ray detectors more information. https://imagine.gsfc.nasa.gov/observatories/technology/gammaray_detectors2.html, 2018. Accessed: 2023-07-20.
- [5] Trevor C Weekes, Michael F Cawley, DJ Fegan, KG Gibbs, AM Hillas, PW Kowk, RC Lamb, DA Lewis, DJ Macomb, NA Porter, et al. Observation of tev gamma-rays from the crab nebula using the atmospheric cherenkov imaging technique. *Astrophysical Journal*, 342:379–395, 1989.
- [6] James Hinton and W. Hofmann. Teraelectronvolt astronomy. Annual Review of Astronomy and Astrophysics, 47, 06 2010. doi: 10.1146/annurev-astro-082708-101816.
- [7] Ctao technology, 2016. URL https://www.cta-observatory.org/project/technology/.
- [8] How c.t.a.o. works, 2016. URL https://www.cta-observatory.org/about/how-ctao-works/.
- [9] D.Y. Nieto, S. Griffiths, Brian Humensky, Philip Kaaret, M. Limon, I. Mognet, A. Peck, A. Petrashyk, Dora Ribeiro, Julien Roussselle, B. Stevenson, V. Vassiliev, Peijiong Yu, and for Consortium. Construction of a medium-sized schwarzschild-couder telescope as a candidate for the cherenkov telescope array: development of the optical alignment system. 09 2015.
- [10] A. Acharyya et. al. The optics and camera system of the schwarzschild-couder telescope and the performance improvement to cta. *Proceedings of Science*. Pending publication.
- [11] I. Heywood, I. Rammala, F. Camilo, W. D. Cotton, F. Yusef-Zadeh, T. D. Abbott, R. M. Adam, G. Adams, M. A. Aldera, K. M. B. Asad, E. F. Bauermeister, T. G. H. Bennett, H. L. Bester, W. A. Bode, D. H. Botha, A. G. Botha, L. R. S. Brederode, S. Buchner, J. P. Burger, T. Cheetham, D. I. L. de Villiers, M. A. Dikgale-Mahlakoana, L. J. du Toit, S. W. P. Esterhuyse, B. L. Fanaroff, S. February, D. J. Fourie, B. S. Frank, R. R. G. Gamatham, M. Geyer, S. Goedhart, M. Gouws, S. C. Gumede, M. J. Hlakola, A. Hokwana, S. W. Hoosen, J. M. G. Horrell, B. Hugo, A. I. Isaacson, G. I. G. Józsa, J. L. Jonas, A. F. Joubert, R. P. M. Julie, F. B. Kapp, J. S. Kenyon, P. P. A. Kotzé, N. Kriek, H. Kriel, V. K. Krishnan, R. Lehmensiek, D. Liebenberg, R. T. Lord, B. M. Lunsky, K. Madisa, L. G. Magnus, O. Mahgoub, A. Makhaba, S. Makhathini, J. A. Malan, J. R. Manley, S. J. Marais, A. Martens, T. Mauch, B. C. Merry, R. P. Millenaar, N. Mnyandu, O. J. Mokone, T. E. Monama, M. C. Mphego, W. S. New, B. Ngcebetsha, K. J. Ngoasheng, M. T. Ockards, N. Oozeer, A. J. Otto, S. S. Passmoor, A. A. Patel, A. Peens-Hough, S. J. Perkins, A. J. T. Ramaila, N. M. R. Ramanujam, Z. R. Ramudzuli, S. M. Ratcliffe, A. Robyntjies, S. Salie, N. Sambu, C. T. G. Schollar, L. C. Schwardt, R. L. Schwartz, M. Serylak, R. Siebrits, S. K. Sirothia, M. Slabber, O. M. Smirnov, L. Sofeya, B. Taljaard, C. Tasse, A. J. Tiplady, O. Toruvanda, S. N. Twum, T. J. van Balla, A. van der Byl, C. van der Merwe, V. Van Tonder, R. Van Wyk, A. J. Venter, M. Venter, B. H. Wallace, M. G. Welz, L. P. Williams, and B. Xaia. The 1.28 ghz meerkat galactic center mosaic. The Astrophysical Journal, 925(2):165, feb 2022. doi: 10.3847/1538-4357/ac449a. URL https://dx.doi.org/10.3847/1538-4357/ac449a.

- [12] L.O'C. Drury F.A. Aharonian and H.J. Völk. Gev/tev gamma-ray emission from dense molecular clouds overtaken by supernova shells. *Astronomy and Astrophysics*, 285:645–647, 1994.
- [13] Science with the Cherenkov Telescope Array. WORLD SCIENTIFIC, feb 2018. doi: 10.1142/10986. URL https://doi.org/10.1142%2F10986.
- [14] S. R. Kelner, F. A. Aharonian, and V. V. Bugayov. Energy spectra of gamma rays, electrons, and neutrinos produced at proton-proton interactions in the very high energy regime. *Phys. Rev. D*, 74:034018, Aug 2006. doi: 10.1103/PhysRevD.74.034018. URL https://link.aps.org/doi/10.1103/PhysRevD.74.034018.
- [15] Tobias Westmeier. Useful equations for radio astronomy, 06 2023. URL https://www.atnf.csiro.au/people/Tobias.Westmeier/tools_hihelpers.php.